Investigation of Pitting in Large-grain Niobium Samples of Different Purity

Gianluigi Ciovati
Thomas Jefferson National Accelerator Facility
Shreyas Balachandran (shreyas@jlab.org)
Thomas Jefferson National Accelerator Facility
D Ens
Old Dominion University
Yi-Feng Su
Oak Ridge National Laboratory
Pashupati Dhakal
Thomas Jefferson National Accelerator Facility
Santosh Chetri
Florida State University
Peter J Lee
National High Magnetic Field Laboratory

Research Article

Keywords: Niobium, Radio-frequency cavities, Surface pitting

Posted Date: May 11th, 2023

DOI: https://doi.org/10.21203/rs.3.rs-2855261/v1

Additional Declarations: No competing interests reported.

Investigation of Pitting in Large Grain Niobium Samples of Different Purity

G. Ciovati[1,2*], S. Balachandran[1], D. Ens[2], P. Dhakal[1], S. Chetri[3], Y. F. Su[3,4] and P. J. Lee[3]

[1]Thomas Jefferson National Accelerator Facility, 12000 Jefferson Ave, Newport News, 23606, VA, USA.
[2]Department of Physics, Old Dominion University, 5115 Hampton Blvd, Norfolk, 23529, VA, USA.
[3]Applied Superconductivity Center, National High Magnetic Field Laboratory, 1800 E Paul Dirac Dr, Tallahassee, 32310, FL, USA.
[4]College of Engineering, FAMU-FSU, 2525 Pottsdamer St, Tallahassee, 32310, FL, USA.

*Corresponding author(s). E-mail(s): gciovati@jlab.org;

Abstract

Niobium samples cut from large-grain discs with residual resistivity ratios ranging between 60 and 300 were mechanically polished and subjected to chemical treatments similar to those applied during the fabrication of superconducting radio-frequency cavities for particle accelerators. Pitting occurred during the chemical treatments and we analyzed the pitting using scanning and transmission electron microscopy as well as TOF-SIMS and light microscopy. We found that the pit density was higher in the samples of lower purity and that electropolishing resulted in the lowest density of pits, regardless of sample purity, compared to buffered chemical polishing. A correlation between high pit density and grains with 100 orientation of the exposed surface was found. However, no strong correlation emerges concerning the dislocation density.

Keywords: Niobium, Radio-frequency cavities, Surface pitting

1 Introduction

Niobium is the material of choice for fabricating superconducting radio-frequency (SRF) cavities for particle accelerators due to its highest critical temperature and upper critical field among elemental superconductors. The standard bulk niobium material used for the SRF-cavity application is specified to have ASTM grain size >5-(corresponds to grain size less than 50 μm) and residual resistivity ratio (RRR) greater than 300 [1].

Recently, SRF cavities were fabricated and processed using large-grain, ingot Nb, making it a viable alternative to the standard Nb [2]. The large-grain Nb discs used for cavity fabrication are directly sliced from a Nb ingot, without additional steps such as forging, rolling, annealing, and grinding used to produce fine-grain discs and therefore allow significant material cost savings. The reduced number of processing steps also reduces the chances of embedding foreign materials into the discs, which could result in a poor rf performance of the SRF cavity. The material purity is another parameter that affects both the cost and performance of SRF cavities. Higher purity is more costly as it requires more refining of the ingot by successive electron beam melting. Lower purity would result in higher cryogenic efficiency of the SRF cavities, as the surface resistance of Nb as a function of the electronic mean free path has a minimum at an RRR-value of ∼20 [3].

Research and development (R&D) efforts on large-grain cavities made from high-purity ingots resulted in several 1.3 GHz, nine-cell cavities reaching a peak surface magnetic field of ∼195 mT at 2.0 K, close to the theoretical limit of superconductivity in Nb [4]. The average quench field of 1.3 - 1.5 GHz single-cell cavities made of medium-purity (RRR ∼ 120-150) ingot Nb was ∼100 mT, even though a quench field of ∼150 mT was recently demonstrated [5, 6], but with a higher quality factor than the same type of cavities made of standard fine-grain Nb, for the same surface treatments [7] . Single-cell cavities made from low-purity (RRR ∼ 60) ingot Nb showed significant surface pitting and a reduced quench field lower than ∼70 mT. Lower RF losses in high-purity large-grain cavities than high-purity fine-grain cavities with similar surface treatments were measured in cryogenic tests of 1.3 GHz nine-cell cavities at KEK [8] and in an accelerating cryomodule at DESY[9].

The RF current flows only within ∼100 nm from the surface, and chemical and mechanical polishing methods are applied to SRF cavities after fabrication to remove surface damage and defects. The amount of material removal necessary to achieve good SRF properties is 100 - 200 μm. One method of material removal is simple chemical etching, referred to as buffered chemical polishing (BCP), in which Nb is etched in a mixture of nitric, hydrofluoric, and phosphoric acid in 1:1:1 or 1:1:2 volume ratios. The phosphoric acid acts as a buffer, reducing the reaction rate. Another chemical removal method is electropolishing (EP), in which a positive polarity is applied to the Nb part, and a negative polarity is applied to a pure aluminum cathode. The electrodes are immersed in a mixture of hydrofluoric and phosphoric acids, a 1:10 volume ratio, and a constant voltage is applied to the electrodes. Another method

to mechanically polish the Nb surface is using centrifugal barrel polishing, in which the cavity is filled with a sequence of finer grinding media and a diluted detergent and rotated at high speed around its axis, which itself is rotating in the opposite direction and parallel to the main shaft, so that the centrifugal force pushes the grinding media against the surface as it rotates

During the R&D on large-grain SRF cavities, a few instances occurred where significant pitting was found on the surface due to the chemical treatment and resulted in poor performance [10–12] . In the past, the occurrence of defects attributed to the chemical processes and limiting the cavity performance has been reported in cavities made of standard Nb as well [13, 14] however, in general, pitting can occur more easily in large crystals and its occurrence has been used in the past as a technique to reveal underlying crystal defects, mainly dislocations [15, 16]. Understanding the conditions that lead to pitting in Nb and their impact on the SRF properties of the material is important to increase the performance of SRF cavities while reducing their cost.

2 Samples preparation and methods

2.1 Sample description, and surface preparation

Four low-purity Nb discs, 2.8 mm thick, 50 mm diameter from OTIC/Ningxia, China, were cut by wire electro-discharge machining (EDM) from the center of four large grain discs 268 mm diameter used to fabricate the cavities discussed in [8]. The samples were labeled JL001-JL004. Six medium purity Nb discs, 3.175 mm thick, 25 mm diameter, were cut by wire-EDM close to the edge of a 318 mm diameter large-grain disc from CBMM, Brazil and labeled F1-F6. Eight high-purity Nb discs, 3 mm thick, 25 mm diameter, labeled 1b-4b and 1a-4a were sliced by wire-EDM from 6 mm thick large grain discs from OTIC/Ningxia, China. The RRR and the impurity concentrations of the different samples were provided by each ingot manufacturer and are listed in Table 1.

Table 1 Samples IDs, RRR and concentration of interstitial impurities (in wt. ppm).

Samples label	RRR	C	O	N	H	Ta
JL001-JL004	60	9	110	30	3	100
F1-F6	118	1	9	8	0.3	1350
1a-4a, 1b-4b	355	7	10	8	2	100

The initial condition of the surface of samples F1-F6, 1a-4a, and 1b-4b is that of the finish given by wire-EDM, corresponding to an average roughness $R_a \sim 1.9$ μm. In contrast, that of samples JL001-JL004 is given by mechanical polishing and BCP done by the Nb supplier, resulting in $R_a \sim 1$ μm. The Nb discs from which pieces JL001-JL004 were cut had also been annealed at

800 °C/2 h in a vacuum furnace. Samples JL002-JL004 were etched by BCP 1:1:2 removing ∼20 μm, followed by mechanical polishing to a mirror finish, $R_a \sim 23$ nm along with samples F1-F5, 1a-4a, and 2 b. The samples were mechanically polished using a Buehler Ecomet 300 grinder-polisher.. After mechanical polishing, ∼10 μm was etched from the surface of samples F1-F5, 1a-4a, and 2 b by BCP 1:1:2, followed by annealing at 800 °C/2 h in a vacuum furnace. For this study, one sample from each purity group was selected to be chemically etched by BCP 1:1:1 or BCP 1:1:2 or electropolished EP, as listed in Table 2. The total material removed by each chemical method was ∼70 μm.

Table 2 Samples were selected for each chemical treatment.

Low Purity	Medium Purity	High Purity	Treatment
JL002	F2	2a	EP
JL003	F3	3a	BCP 1:1:2
JL004	F4	4a	BCP 1:1:1

Chemical etching by BCP was done by directly immersing a basket with each group of samples into a container with the acid mixture. The acid temperature was maintained at ∼15 °C with a water bath, and the basket was moved inside the container with the acid to maintain a slow flow of acid over the samples' surface. The samples were mounted in a small cell filled with the acid mixture for the EP. A constant voltage of 10 V was applied between the Nb samples and the aluminum cathode, resulting in a current density of ∼50 mA/cm^2. The temperature was kept at ∼17 °C with a water bath, and a magnetic stirrer was used to agitate the acid mixture. The amount of material removed was determined by the weight change of one of the samples. The measured etched rates were 5.7 μm/min and 2.1 μm/min for BCP 1:1:1 and 1:1:2, respectively, and 0.6 μm/min for EP.

2.2 Microscopy and Micro-analysis

Sample microstructures were evaluated in a Zeiss 1540 EsB scanning electron microscope (SEM). Grain orientations of the various large grains were obtained using orientation imaging microscopy (OIM). The orientation imaging was performed in the same SEM as above, equipped with an EDAX-Hikari high-speed OIM camera. An electron beam energy of 15 keV and a step size of 100-500 nm was used to identify the crystallographic orientations. At these step sizes, the angular precision of the instrument is about 0.1°. The angular accuracy of the OIM system is within 2° for the analysis. The MTEx [17, 18], MATLAB® plugin was used to plot the orientations on the inverse pole figure (IPF).

The microstructure of select high-purity and low-purity samples was characterized using a JEOL ARM 200 F transmission electron microscope (TEM) operated at 200 kV. TEM foils were prepared from low-purity sample JL003

and high-purity sample 3a in the grains with the highest pit density. The TEM specimens were prepared using focused ion beam (FIB) milling. Before milling, a strap of platinum (3-μm wide, 20-μm long, and 1-μm thick) was deposited on the sample to protect the surface over the area of interest during high-energy gallium ion (Ga^+) bombardment. The FIB'ed lamella (2μm $\times$ 20 μm $\times$ 12μm) was lifted and placed on a TEM grid. The lamella was further milled on both sides to form a narrow window sufficiently electron transparent (100 nm) to allow detailed images to be recorded. It was observed that the Ga ion bombardment could cause damage to the surface layers, which could be easily removed by chemical removal using the BCP 1:1:2 solution. All TEM bright-field images were taken at 100 k magnification.

3 Samples analysis

3.1 Pit density, shape, and size

Pictures of the whole samples after they have been processed, as listed in Table 2, are shown in Fig. 1. The grain boundaries are highlighted in yellow, and a letter was used to identify each grain. The density of the pits was measured using a high-resolution optical digital microscope (HIROX KH-3000VD) using the instrument's software to create a grid overlay. A magnification of 140 times was typically adequate to see the pits. The grid size was chosen to be 1 mm x 1 mm, and pits within up to fifty one mm^2 boxes were counted. The average pit density for all the grains for each sample is shown in Fig. 2. Some characteristic images of the pitting patterns in some of the sample are shown in Fig. 3. The shape of the pits observed on different grains in different samples was examined with a scanning electron microscope (TESCAN VEGA3), and it is shown in Fig. 4.

Information regarding the size and depth of the pits was obtained by scanning 2 $\times$ 2 mm regions of the sample with a 3D surface profiler (KLA-Tencor) and using the instrument's software cross-section tool and cursors. Histograms of the depth and size for all the samples are shown in Figs. 5 and 6.. The data do not follow a normal distribution, and only a limited number of counts are available for samples with lower pit densities. The depth is small compared to the thickness of the material removed. The measured pits depths for the BCP 1:1:1 polished low-purity Nb were significantly higher than for the other samples, whereas the medium purity material had the shallowest pits for all treatments (Fig. 5b), and yet their widths tended to be greater (Fig. 6b).

3.2 Impurities depth profile

To determine whether there is a significant difference in the distribution of interstitial impurities among different samples and grains, regions of samples 3a, F3, JL003, and JL002 shown by circles in Fig. 1 were analyzed by time-of-flight secondary ion mass spectrometry (ION TOF, TOF SIMS V) at North Carolina State University. A low energy Cs^+ beam with 20 nA current was

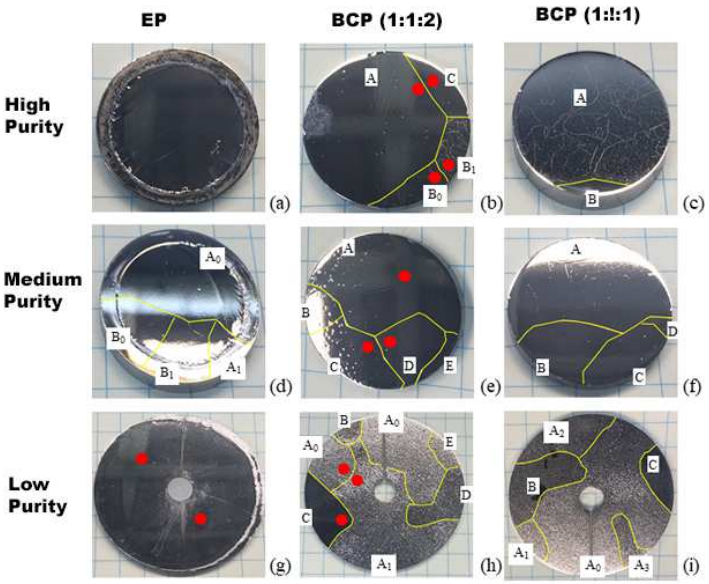

Fig. 1 Photographs of the nine samples used for this study. Top row: 2a, 3a and 4a, (a)-(c) respectively. Middle row: F2, F3, and F4, (d)-(f), respectively. Bottom row: JL002, JL003 and JL004 (g)-(i), respectively. The yellow lines delineate grain boundaries, and letters identify different orientations within a sample. The red dots show the approximate location of the regions analyzed with time-of-flight secondary ion mass spectroscopy

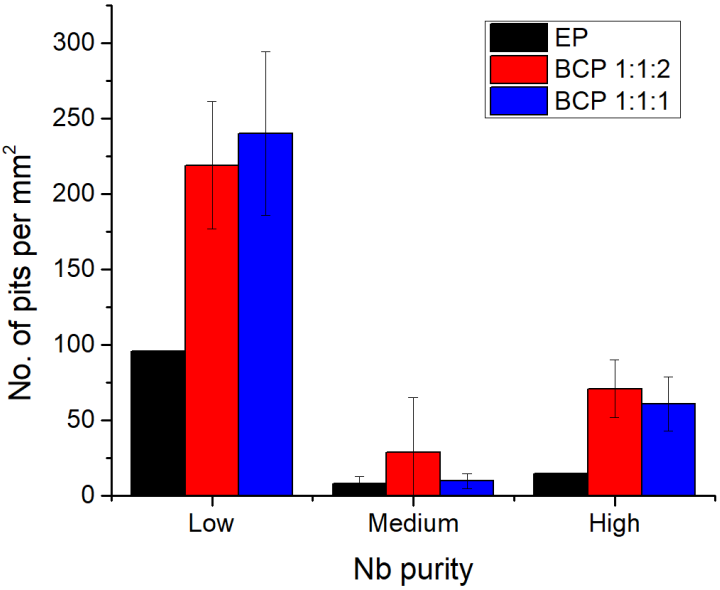

Fig. 2 Pit density averaged over the whole sample for each Nb purity, for each of the applied surface chemical treatments.

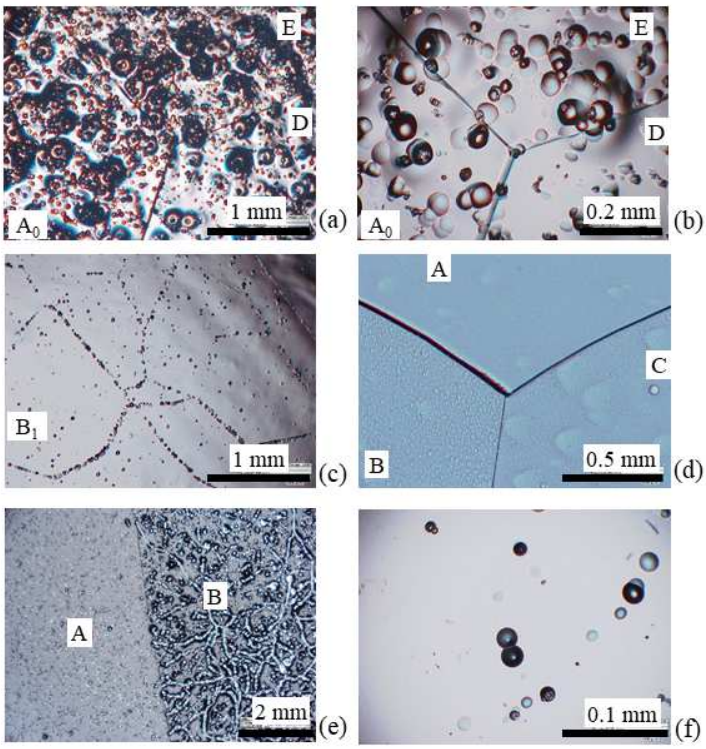

Fig. 3 Characteristic images of the surfaces of some of the samples: (a)-(b) JL003 at different magnifications (c) 3a, (d) F4, (e) JL004, and (f) JL002. Letters identify different grain orientations.

used to create a 120 μm by 120 μm area, and the middle 50 μm by 50 μm site was analyzed using about 0.3 pA Bi_3^+ primary ion beam. The sputtering depth was 1 μm. Both regions with pits and without pits were analyzed. The results showed no significant differences, given the instrument's resolution, in the C, N, O, and F depth profiles among different samples, grains, or pit versus flat regions. The only difference was that the concentration of hydrogen is about a factor of ten higher in JL003 and JL002 samples than in samples 3a and F3, likely because of the mechanical polishing which was not followed by a vacuum annealing in those samples. 3D ion distributions were acquired in (50×50) mm^2 areas that included pits for samples 3a, JL002 and JL003. Evidence for higher impurities concentration in a pit than in the surrounding region was seen most clearly in sample JL003-A0, as shown in Fig. 7.

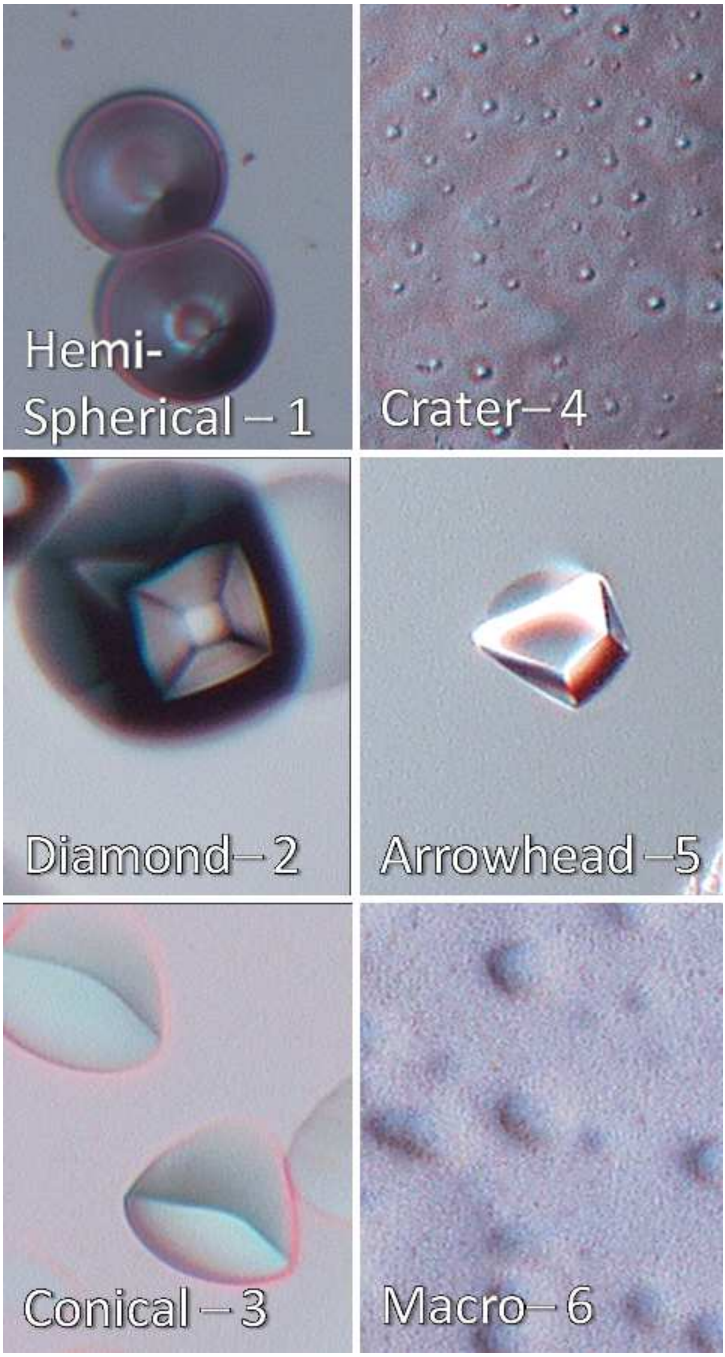

Fig. 4 Characteristic shapes of the pits observed in the different samples.

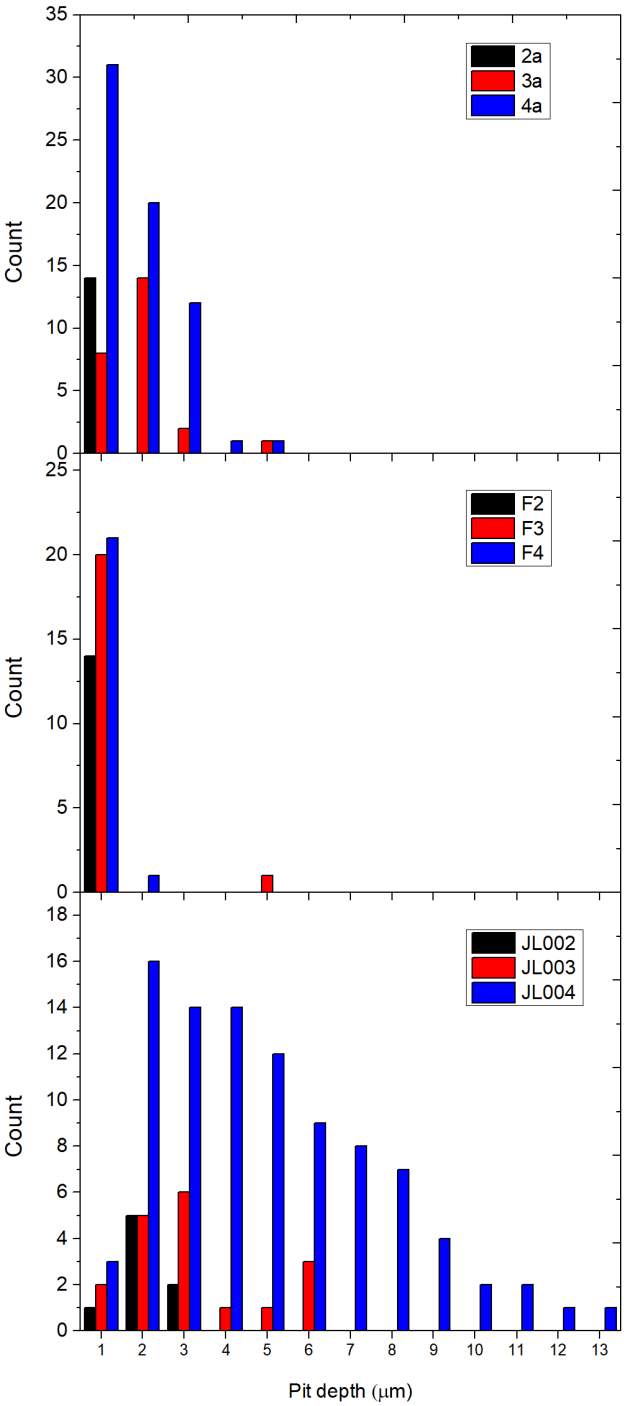

Fig. 5 Distribution of pits' depth in high-purity samples (top), medium-purity samples (middle), and low-purity samples (bottom).

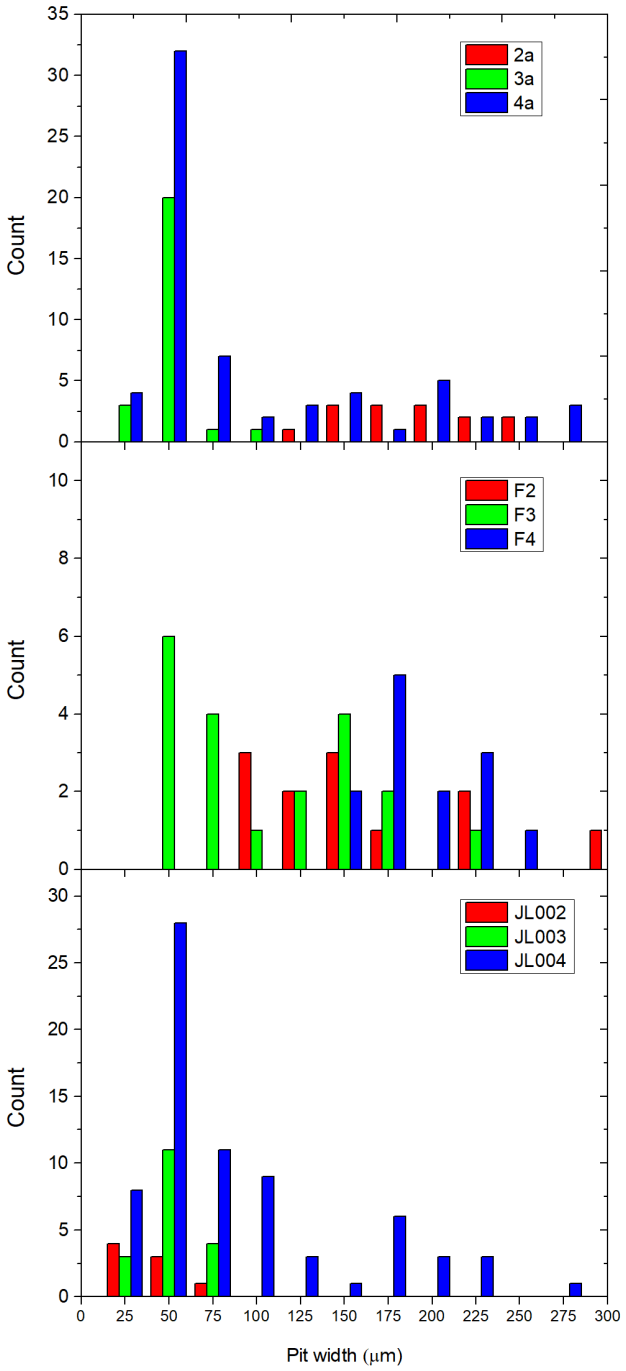

Fig. 6 Distribution of pits' size in high-purity samples (top), medium-purity samples (middle), and low-purity samples (bottom).

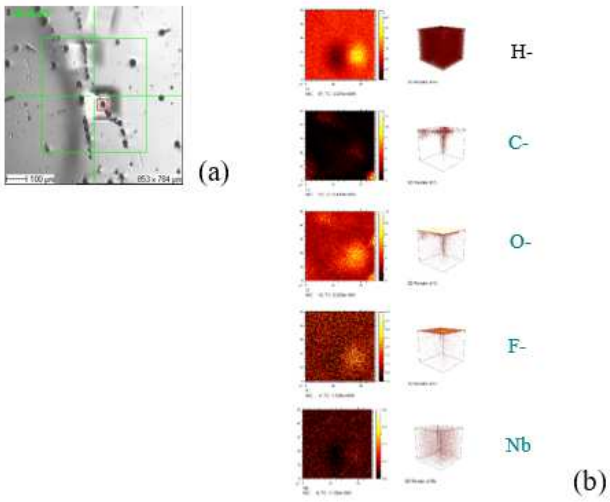

Fig. 7 (a) SEM image of sample JL003: 3D ion distributions of selected impurities were acquired from the region within the red box and are shown in (b).

3.3 Relationship between grain orientations and pit density

To determine if there are orientation relationships between the density of etch pits versus the surface normal orientation of the grains, OIM was performed on all the grains, and the pit density was correlated to the grain orientations. Figure 8 indicates the inverse pole figure in the direction normal to the sample's surface. The size of the symbols on the IPF indicates the pit density; the higher the pit density, the more significant is the symbol. Out of the analyzed 26 orientations on various Nb samples, we find high pit density correlations associated with the surface having the [001] normal, as indicated in Fig. 8.

The summary of the pit densities and sample orientations is presented in Table 3. The following observations can be further made from the available data. In general, EP leads to lower pit densities than BCP. It is known that BCP leads to extensive etching, and from the IPF in Fig. 8, it is clear that there is a preferential etching rate with orientation. EP of low purity Nb leads to pit densities as high as 96 mm^{-2}, as seen in grain A of sample JL002 which is concerning. BCP (1:1:1) leads to significantly lower pit densities in medium-purity samples compared to BCP (1:1:2).

3.4 Patterns in etch pitting and microstructural dependence

Some patterns appear in etch pitting on the LG Nb surfaces, indicating orientation relationships. Figure 9 shows some representative regions of low-purity sample JL003 and high purity sample 3a, which have both undergone BCP

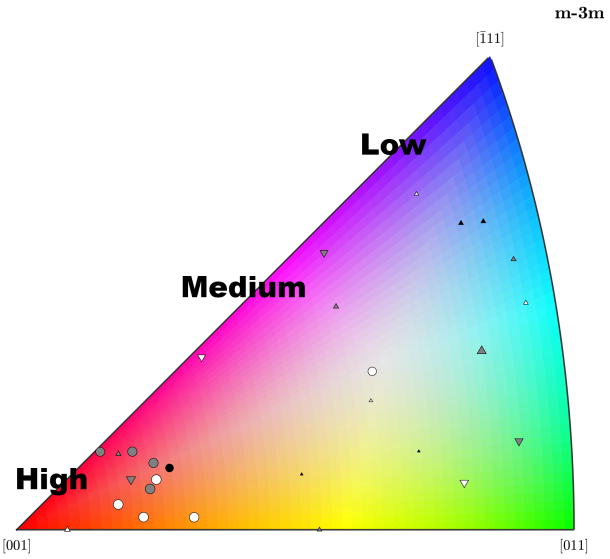

Fig. 8 Inverse pole figure (IPF) representing the analyzed orientations in the surface normal direction (z-axis) for various Nb purities: High purity (downward triangle), Medium Purity (upward triangle), and Low purity (circle). The colors of the markers represent the chemical processing namely: EP (black), BCP (1:1:2) (grey), and BCP (1:1:1).

1:1:2. Triangular pits could be found in both high-purity and low-purity samples. Analysis of the directions from the OIM images indicates that triangular pits have $< 110 >$ directions along the triangles, although the orientation of the surface plane normals can vary. Most pits get rounded which could be due to longer etching times and rates. EBSD of the grains with etch pits could not reveal reliable misorientation information due to the surface roughness created by the pits. To explore if there are any differences in etch pit density due to dislocation density, we EDM cut a quarter of a disc of JL003, which was characterized, and mechanically polished the disc to remove 100 μm, and then heat treated the sample at 1000 °C/3 h in a vacuum furnace. After the heat treatment, the same BCP 1:1:2 recipe (Table 1) was used to etch about 70 μm from the sample surface. High-temperature heat treatment of 1000 °C/2 h was found to be sufficient to recover dislocations introduced by the uniaxial strain of single and bi-crystal Nb samples [10]. Figure 10 indicates representative images of etch pits in JL003 before and after the 1000 °C/3h followed by BCP 1:1:2. There was no significant change in the pit density: the initial pit density of the sample was 196 mm^{-2}, whereas it was 184 mm^{-2} after the 1000 °C/3 h and subsequent BCP. The possible influence of local misorientations caused by dislocations were further explored by TEM analysis. To investigate if there were any differences in the dislocation density or structure, we chose grains with the highest pit density after BCP1:1:1. In the low purity (grain

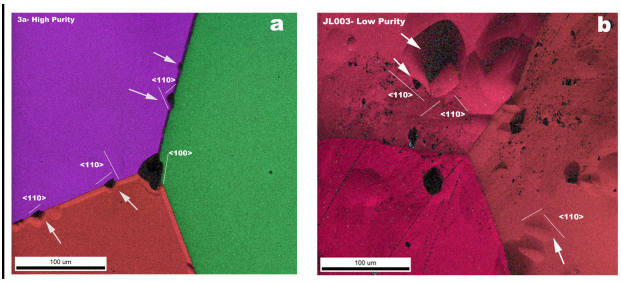

Fig. 9 OIM images of high purity sample 3a (a), and low purity sample JL003 (b) both etched by BCP 1:1:2. There is a significant difference in pit density density depending on the purity of the sample. However, the edges of the pits that are triangular share similarities that show that the directions of the triangular edges are $< 110 >$.

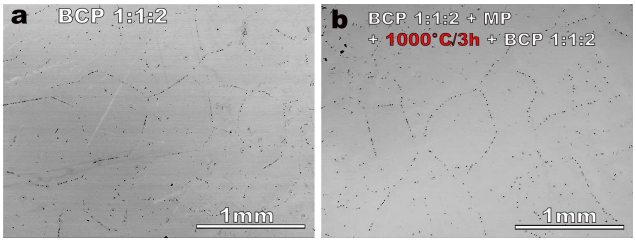

Fig. 10 (a) Back-scatter SEM images of sample JL003-low purity Nb sample, orientation A0, after an initial BCP 1:1:2 , and (b) after 100µm removal of previous surface by mechanical polishing (MP) followed by a high temperature heat treatment at 1000 °C/3h and 70 μm removal by BCP 1:1:2. The pit densities in the two cases are not very different and are 180-200 mm^{-2} irrespective of the heat treatment cycle.

E in sample JL003) and high purity (grain A in sample 3a), the microstructure was analyzed using a TEM. Bright-field (BF) images in Fig. 11indicate representative regions of the surveyed large grains.

There are dislocations present in the sample even after heat treatments in both low and high purity samples. The dislocations have not formed a network structure indicating that these are annealed structures and represent in-grown dislocation structures that are expected in the extensive grain material. No variations in the O, N levels could be picked up from these sections using EDS on the TEM. Based on six regions surveyed in each of the samples, the dislocation densities were calculated by counting the length of the dislocation segment and dividing it by the interaction volume. The dislocation density was estimated to be 2.5 $\times 10^{13}$ m^{-2} for the high-purity sample and 4×10^{13} m^{-2} for the low purity sample. From this analysis there was no difference in the dislocation density between the two samples or chemistry differences that could be picked up with the TEM analysis between the low purity and high purity samples.

Table 3 Summary of orientation pit density correlations in Nb of varying purity, subjected to chemical, and electropolishing.

Sample ID	Purity	Treatment	Orientation in Euler angles			Pit density (mm^{-2})
			ϕ_1	Φ	ϕ_2	
2a	High	EP				
3a-A		BCP 1:1:2	292	147	318	54
3a-B		BCP 1:1:2	178	81	274	98
3a-C	High	BCP 1:1:2	281	41	10	63
4a-A		BCP 1:1:1	323	144	276	73
4a-B		BCP 1:1:1	68	160	43	48
F2-A0		EP	278	113	8	11
F2-A1		EP	118	113	220	11
F2-B0		EP	359	122	187	4
F2-B1		EP	196	157	259	4
F3-A		BCP 1:1:2	359	140	339	94
F3-B		BCP 1:1:2	310	115	341	14
F3-C	Medium	BCP 1:1:2	298	156	90	10
F3-D		BCP 1:1:2	54	82	354	13
F3-E		BCP 1:1:2	97	110	228	13
F4-A		BCP 1:1:1	146	30	290	3
F4-B		BCP 1:1:1	77	45	336	10
F4-C		BCP 1:1:1	1	90	184	17
F4-D		BCP 1:1:1	125	138	220	8
JL002-A		EP	95	167	338	96
JL003-A0		BCP 1:1:2	102	169	304	220
JL003-A1		BCP 1:1:2	216	171	47	196
JL003-D		BCP 1:1:2	175	12	334	221
JL003-E		BCP 1:1:2	75	11	73	281
JL004-A0	Low	BCP 1:1:1	336	82	182	266
JL004-A1		BCP 1:1:1	167	80	269	266
JL004-A2		BCP 1:1:1	345	101	4	266
JL004-B		BCP 1:1:1	146	31	294	132
JL004-C		BCP 1:1:1	236	76	1	246

4 Discussion

The following main results can be extracted from the experimental data presented in the previous sections:

1. The low-purity samples have the largest pit density, irrespective of the chemical treatment, either BCP or EP.
2. EP results in the lowest pit density and in shallower, wider pits compared to BCP.
3. A correlation between the pit density and grain orientation was found for the same purity level: orientations that have a {100} surface normal always lead to higher pitting than {111} or {110} normal orientations.

The surface analysis methods available for this study did not have a resolution of ∼1 at. ppm. necessary to determine whether there is any significant

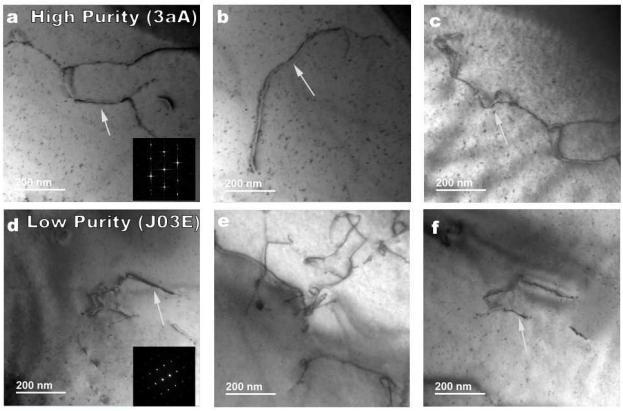

Fig. 11 BF-TEM images indicating dislocations in the form of dark contrast in large grain Nb samples. a)-c) correspond to high purity sample 3a-A, and d)-f) correspond to low purity sample JL003-E. Dislocations are apparent in both materials, and the average dislocation density does not vary much with purity and it is $\sim 10^{13}$ m^{-2}.

systematic difference in the low concentration of interstitial impurities in different grains of samples of different purity. We found some evidence of higher concentration of impurities (O, C, H, F) within a pit. These results are consistent with those in Ref. [19] higher surface O and C concentrations were found within a pit, along with niobium hydrides and chain-type hydrocarbons. Etch pitting follows crystallographic orientations, triangular pits always have a ¡110¿ edge irrespective of the orientation. The combination of some surfaces having a better response to etch pitting and crystallographic orientations along etch pits may indicate some orientations with {111} or {110} normals that could potentially lead to the best polished surfaces even after chemical polishing. The analysis of pitted large-grain Nb samples cut from an SRF cavity showed some correlation between the dislocation density inferred from OIM maps and pit density. The TEM images of high and low purity samples reported here indicate similar density of dislocations. The values are consistent with those of metals solidified after purification in an electron beam melting furnace [20]. The difference between the samples analyzed for this study and those of Ref. [19] is that the latter were subjected to plastic deformation during the deep-drawing of the cavity half-cells. The OIM maps used to determine the grain orientations in this work could not be used to study the dislocation density since they were measured with a too-large step interval of 1 μm. It is also known that the nature of oxide is dependent on the orientation of the surface normal. The oxide formed on Nb(100) is very different from Nb(110) and Nb (111). The surface oxide formed on the (110), and (100) Nb surface are ordered, whereas the (111) oriented surface forms a disordered oxide [21, 22]. In a bcc metal such as Nb, the (110) plane is the most closely packed, and the ¡111¿ direction is the closed packed direction. BCP leads to etching and we do not have a control over polishing versus etching during chemical polishing. It is possible that local variations in chemistry in the low purity material due to

O, H, N could create local differences in polishing and etching rates depending on the local distribution of interstial elements. Since the Nb is electron beam melted one would assume that the interstitial distribution is random except in regions around grain boundaries. However, we observed no preferential etching in the LP or HP material around GB's. One of the reasons for increased pitting in the LP case versus the HP case for the same chemical solution could be explained by this hypothesis: interstitial elements get trapped about dislocations and lead to higher rate of etching [9]. Our results strengthen this hypothesis. The specific example here is that HP and LP samples have similar dislocation densities of the order of $10^{13}m^{-2}$, they have vastly different pit densities. for example 3a-A has a pit density of 54 mm^{-2} versus JL003-E has a pit density of 281 mm^{-2}. The most common pitting corrosion type is local dissolution following the breakdown of an otherwise protective passive film. Furthermore, pits almost always initiate at some chemical or physical inhomogeneity at the surface [23]. TEM measurements on single-crystal Nb samples showed that the {100} orientation has the thinnest oxide [24], which may result in easier local breakdown of the oxide at defect locations. Higher surface fluorine concentration at the surface was also found in Nb with {100} orientation than in {110} or {111} [25]. Pitting can also occur during active dissolution if some regions of the samples dissolve faster than the rest of the surface. The 100 orientation is expected to have the lowest etch rate because it has a low surface energy, although it could depend on the type of etchant and environmental conditions. An experimental study showed the {110} orientation to have the fastest etch rate and the {111} orientation the lowest [26]. The fact that EP is a diffusion-limited reaction making it insensitive to grain orientation, might explain the lower pit density obtained by EP than BCP.

5 Conclusion

The analysis of Nb samples cut from large-grain discs of different purity used for the fabrication of SRF cavities and treated using the same chemical material removal methods used in processing the cavities show the presence of pits. EP results in the lowest pit density. A correlation was found between higher pit density and the {100} crystal orientation. However, no clear correlation was found between the dislocation density and the density of pits. The role of the interstitial impurities, with the oxygen concentration being the main difference among samples of different purity, on pit formation is unclear and would require further studies. We plan to further investigate the impact of grain orientation and dislocation density on underformed samples cut from standard fine-grain high-purity Nb. Since it is not feasible to accurately control the grain orientations within large Nb ingots, this study suggests EP as a better cavity surface treatment method to minimize the occurrence of pits which can limit the performance of SRF cavities.

Acknowledgments. We acknowledge Hongyun Zhao of OTIC/Ningxia for providing the high-purity Nb material and G. R. Myneni for providing the

medium-purity Nb material. We would like to acknowledge Olga Trofimova and the College of William and Mary Applied Research Center Core Labs for providing access and helping with the optical microscopy and Elaine Zhou at the Analytical Instrumentation Facility at North Carolina State University for ToF-SIMS measurements. This manuscript has been authored by Jefferson Science Associates, LLC under U.S. DOE Contract No. DE-AC05-06OR23177. The U.S. Government retains a non-exclusive, paid-up, irrevocable, world-wide license to publish or reproduce this manuscript for U.S. Government purposes. This work was supported by the U.S. Department of Energy (Award Numbers DE-SC0009962 and DE-SC0009960). A portion of this work was performed at the National High Magnetic Field Laboratory, which is supported by National Science Foundation Cooperative Agreement No. DMR-1157490 (-2017) DMR-1644779 (2018-) and the State of Florida.

Author contributions. GC was responsible for the conceptualization, funding acquisition for the project, DE,SB, SC were involved with the investigation, GC, SB, and PD were involved with generating the methodology, visualization, formal analysis and the writing of the original draft. PJL contributed towards funding acquisition, and methodology development for the electron microscopy work. All the authors were involved with the review and editing.

Conflicts of interest or competing interests. The authors declare no conflict of interest or competing interests.

Data and code availability. Data will be provided based on request.

Supplementary information. Not applicable

Ethical approval. Not applicable

References

[1] W. Singer, A. Brinkmann, D. Proch, and X. Singer, Quality requirements and control of high purity niobium for superconducting RF cavities, Phys. C Supercond. 386 (2003) 79–384.

[2] P. Kneisel *et al.*, Review of ingot niobium as a material for superconducting radiofrequency accelerating cavities, Nucl. Instrum. Methods Phys. Res. Sect. Accel. Spectrometers Detect. Assoc. Equip. 774 (2015) 133–150.

[3] J. Halbritter, On surface resistance of superconductors, Z. Für Phys., 266(3) (1974) 209–217.

[4] W. Singer *et al.,* Development of large grain cavities, Phys. Rev. Spec. Top. Accel. Beams, 16(1) (2013) 012003.

[5] H. Shimizu *et al.,* Fabrication and Evaluation of Superconducting Single-Cell Cavities Manufactured Using Various Materials and Methods, IEEE Trans. Appl. Supercond. 27(7) (2017) 1–14.

[6] P. Dhakal, G. Ciovati, and G.R. Myneni, Evaluation of High Performance Large Grain Medium Purity SRF Cavity From KEK, in Proc. SRF'19, Dresden, Germany, (2019) 415-418.

[7] G. Ciovati, P. Dhakal, and G. R. Myneni, Superconducting radio-frequency cavities made from medium and low-purity niobium ingots, Supercond. Sci. Technol., 29 (6) (2016) 064002.

[8] T. Dohmae *et al.,* Investigation on 1, 3 and 9-cell SRF elliptical cavities made of large grain niobium, in Proc. 19^{th} Int. Conf. RF Superconductivity, (2019) 1213–1215.

[9] J. Sekutowicz *et al.*, Research and development towards duty factor upgrade of the European X-Ray Free Electron Laser linac, Phys. Rev. Spec. Top. Accel. Beams, 18 (5)(2015) 050701.

[10] X. Zhao, G. Ciovati, and T. R. Bieler, Characterization of etch pits found on a large-grain bulk niobium superconducting radio-frequency resonant cavity, Phys. Rev. Spec. Top. Accel. Beams, 13(12) (2010) 124701.

[11] T. R. Bieler *et al.*, Deformation mechanisms, defects, heat treatment, and thermal conductivity in large grain niobium, AIP Conf. Proc. 1687(1) (2015) 020002.

[12] J. Mondal, G. Ciovati, P. Kneisel, K. C. Mittal, and G. R. Myneni, Design, fabrication, RF test at 2 K of 1050 MHz, β=0.49 single cell large and fine grain niobium cavity, J. Instrum.,6(11) (2011) T11003.

[13] M. S. Champion *et al.*, Quench-Limited SRF Cavities: Failure at the Heat-Affected Zone, IEEE Trans. Appl. Supercond. 19(3) (2009) 1384–1386.

[14] L. D. Cooley *et al.*, Impact of Forming, Welding, and Electropolishing on Pitting and the Surface Finish of SRF Cavity Niobium, IEEE Trans. Appl. Supercond. 21(3) (2011) 2609–2614.

[15] P. R. V. Evans, Dislocation etch pit studies in annealed and deformed polycrystalline niobium, J. Common Met. 6(4) (1964) 253–265.

[16] B. C. Cai, A. Dasgupta, and Y. T. Chou, Etch pits on single crystals and bicrystals of niobium, J. Common Met.90(1) (1983) 37–47.

[17] D. Mainprice, F. Bachmann, R. Hielscher, and H. Schaeben, Descriptive tools for the analysis of texture projects with large datasets using MTEX:

strength, symmetry and components, Geol. Soc. Lond. Spec. Publ. 409(1) (2015) 251–271.

[18] R. Hielscher and H. Schaeben, A novel pole figure inversion method: specification of the MTEX algorithm, J. Appl. Crystallogr. 41(6) (2008).

[19] C. Cao *et al.*, Detection of surface carbon and hydrocarbons in hot spot regions of niobium superconducting rf cavities by Raman spectroscopy, Phys. Rev. Spec. Top. Accel. Beams, 16(6) (2013) 064701.

[20] V. G. Glebovsky and V. N. Semenov, Growing Single Crystals of High-Purity Refractory Metals by Electron-Beam Zone Melting, High Temp. Mater. Process. 14(2) (1995) 121–130.

[21] K. Zhussupbekov *et al.*, Oxidation of Nb (110): atomic structure of the NbO layer and its influence on further oxidation, Sci. Rep. 10(1) (2020) 1–9.

[22] R. D. Veit, N. A. Kautz, R. G. Farber, and S. J. Sibener, Oxygen dissolution and surface oxide reconstructions on Nb(100), Surf. Sci. 688 (22019) 63–68.

[23] G. S. Frankel, Pitting Corrosion of Metals: A Review of the Critical Factors, J. Electrochem. Soc. 145(6) (1998) 2186.

[24] A. D. Batchelor, D. N. Leonard, P. E. Russell, F. A. Stevie, D. P. Griffis, and G. R. Myneni, TEM and SIMS Analysis of (100), (110), and (111) Single Crystal Niobium, AIP Conf. Proc. 927(1) (2007) 72–83.

[25] X. Singer, K. Kowalski, and W. Singer, Large Grain DESY Cavities and Crystallographic Orientation of the Niobium Discs, in 16^{th} International Conference on RF Superconductivity (2013) no. DESY-2014-00378.

[26] L. Zhao, C. E. Reece, and M. J. Kelley, Genesis of Topography in Buffered Chemical Polishing of Niobium for Application to Superconducting Radiofrequency Accelerator Cavities, in 18^{th} International Conference on RF Superconductivity, JACoW, Lanzhou, China, 2017.